

BRIEF COMMUNICATION OPEN



Seasonal forecasts of the world's coastal waterline: what to expect from the coming El Niño?

Julien Boucharel^{1,2}, Rafael Almar¹ and Boris Dewitte^{3,4,5}

The central-eastern tropical Pacific is currently significantly warmer than normal, and the likelihood of a strong El Niño developing by early 2024 is 75–85%, according to the National Weather Service's Climate Prediction Center. Disruptions in ecosystem services and increased vulnerability, in particular in the coastal zones, are expected in many parts of the world. In this comment, we review the latest seasonal forecasts and showcase the potential for predicting the world's coastlines based on data-driven modeling.

npj Climate and Atmospheric Science (2024)7:37; <https://doi.org/10.1038/s41612-024-00570-z>

BEYOND THE CRYSTAL BALL: STATE-OF-THE-ART SEASONAL EL NIÑO FORECASTS

El Niño Southern Oscillation (ENSO) is one of the most significant climate phenomena on Earth, with far-reaching impacts on weather patterns, agriculture, ecosystems and socio-economic systems¹. Accurate forecasting of ENSO events is critical for governments, industries and communities to prepare for and respond effectively to the risks and opportunities they present². A better understanding of oceanic and atmospheric dynamics, together with increased computing power, has led to significant advances in coupled general circulation models, which can now realistically simulate ocean-atmosphere interactions, allowing a better representation of ENSO dynamical processes and enhanced predictive capabilities over longer lead times^{3,4}. In addition, the use of ensemble forecasts has become standard practice in ENSO forecasting, allowing for uncertainties in the model physics and initial state data to be taken into account, and therefore leading to significantly improved forecasts^{5–7}.

Based on such state-of-the-art model resource for seasonal predictions, we present the tropical Pacific forecasts for the upcoming months from the North American Multi-Model Ensemble (NMME) project (Table 1), a forecast system that includes models from operational centers in the USA and Canada⁸. Figure 1 shows the multi-model ensemble forecasts of monthly interannual sea surface temperature (SST) anomalies, initialized on October 1st, for the period October 2023 to May 2024. Large SST anomalies along South America and extending into the eastern equatorial Pacific reveal an Eastern Pacific El Niño pattern already strongly established in the boreal fall (Fig. 1a, b). In fact, the SST anomalies along the Peruvian coast have already been so large even earlier this spring, reaching 6 °C above climatology on 4 April 2023 according to data from the Multiscale Ultrahigh Resolution Sea Surface Temperature project, that Peru's National Meteorological and Hydrological Service declared the area to be experiencing a coastal El Niño as early as March 2023⁹. Warm anomalies in the far eastern tropical Pacific are expected to persist until the end of the boreal autumn (Fig. 1a), when they begin to move away along the equator into the central Pacific (Fig. 1b, c), consistent with the westward propagating residual annual SST mode in this region¹⁰ and also a common feature of the “canonical” El Niño (i.e., starting in the east and propagating westward¹¹). This leads to a pattern of

SST anomalies more similar to the Central Pacific El Niño type in the heart of the boreal winter (Figure 1d–f). Finally, the models predict that SST anomalies across the equatorial Pacific will finally begin to decline significantly by the end of the winter and into the following spring (Fig. 1f, g), returning to near-neutral values by May 2024 (Fig. 1h). Figure 1i, j shows the predicted temporal evolution of the two classical ENSO indices, Niño3 and Niño4 (see definition in Fig. 1 caption) for the individual NMME models, the multi-model ensemble average and the observed indices for the two strongest El Niño episodes on record, the 1997–98 and 2015–16 events as a benchmark for assessing the amplitude of the current event. Both indices are predicted to peak in early winter, with values well above the El Niño threshold in both the eastern and western Pacific, meaning that the upcoming event is expected to be a mix between the eastern and central Pacific modes^{12,13}, comparable to the 2015–16 event, although with a weaker imprint in the eastern part of the basin.

ONE OF EL NIÑO'S FOOTPRINTS: RESHAPING AND FLOODING THE WORLD'S COASTLINES

Numerous studies investigating the effects of El Niño have shown that it has a profound impact on regional climates and ecosystems, extending well beyond its primary area of influence. These widespread impacts include various aspects such as disease incidence¹⁴, susceptibility to mass coral bleaching¹⁵, changes in fire¹⁶, in fish abundance and distribution¹⁷, and even its effects on national economies, sectors, and food security^{18,19}. Because 600 million people live in coastal areas less than 10 meters above sea level, the links between ENSO and coastal vulnerability have been studied extensively^{20–30}. In particular, a recent study has built on the many theoretical breakthroughs in understanding the complex and diverse regimes of ENSO and their teleconnections³¹, including their remote effects on drivers of coastal variability (e.g., waves, sea level, and rivers)^{32–34}, to formulate a climate-based conceptual model of global coastal waterline evolution³⁵ taking advantage of a new data resource allowing to assess multi-year fluctuations in its position.

The Earth's coastal waterline is a remarkably dynamic interface over a wide range of timescales, and even small shifts in its position can induce coastal erosion and increased flooding risks

¹LEGOS, Université de Toulouse III, (CNRS/IRD/UPS), Toulouse, France. ²Department of Atmospheric Sciences (University of Hawaii at Manoa), Honolulu, HI, USA. ³CECI, Université de Toulouse III, CERFACS/CNRS, Toulouse, France. ⁴Centro de Estudios Avanzados en Zonas Áridas (CEAZA), Coquimbo, Chile. ⁵Center for Ecology and Sustainable Management of Oceanic Islands (ESMOI), Departamento de Biología Marina, Facultad de Ciencias del Mar, Universidad Católica del Norte, Antofagasta, Chile. ✉email: julien.boucharel@ird.fr; rafael.almar@ird.fr

thus having pronounced economic and societal impacts. As an illustration, Fig. 2a shows the amplitude of seasonal variations in global waterline position from a monthly dataset of satellite-

Models	Max lead	Forecast period
CanCM4i	9 months	October 2023-June 2024
GEM-NEMO	-	-
GFDL-SPEAR	-	-
NASA-GEOS2S	-	-
NCEP-CFSv2	-	-
NCAR-CCSM4	-	-
NCAR-CESM1	-	-

derived waterlines spanning the period 1999 to 2019. These variations range from 0 to ~25 m and are generally small in the tropics and large in the extratropics, especially below the mid-latitude storm tracks, reflecting the amplitude of the seasonal change in wind-driven sea level and wave activity, which are the dominant contributors to the seasonal variation of coastal water level and thus the waterline position. The recently proposed conceptual model³⁵ of waterline position uses as predictors different ENSO indices (i.e., Niño3, Niño4 and their respective annual combinations^{35,36}) and other indices representative of basin wide modes of climate variability to simulate the interannual evolution of its position. After training this model using historical values of the climate indices and the satellite-derived waterline positions, it is used in forecast mode using the climate indices predicted by the NMME system. Figure 2b presents the model ensemble forecasts at the predicted peak of the upcoming El Niño (November 2023-January 2024 mean). Notably, the ENSO indices convey the greater source of predictability, while other climate modes (the Indian Ocean Dipole, Southern Annular Mode and

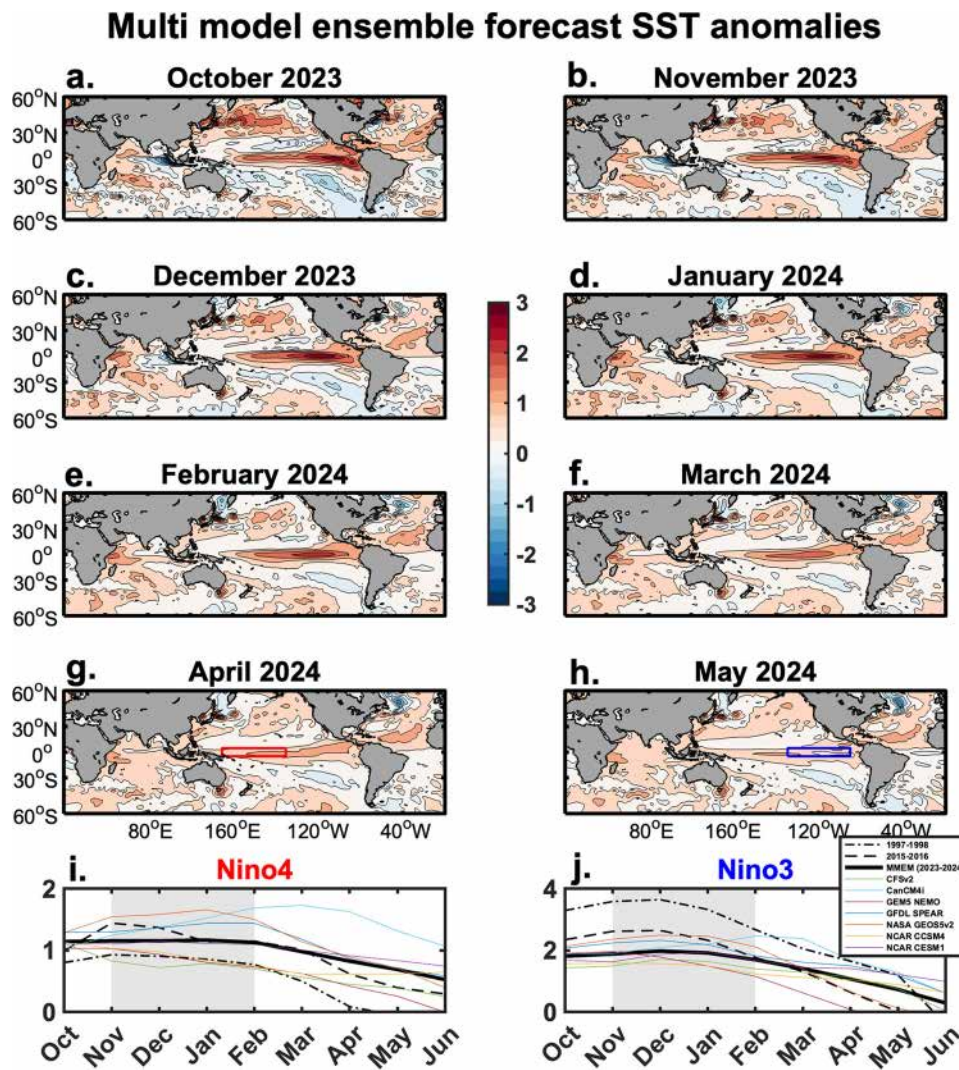


Fig. 1 El Niño forecasts. North American Multi-Model Ensemble (NMME) average forecasts of monthly interannual sea surface temperature (SST) anomalies (in °C), initialized on October 1st, for the month of October (a), November (b), December (c) 2023, January (d), February (e), March (f), April (g) and May (h) 2024 (contours are every 0.5 °C). Predicted temporal evolution of Niño4 (i) and Niño3 (j) (SST anomalies averaged over the region [5°N-5°S, 150°W-160°E-150°W] delineated in red in (g) and [5°N-5°S, 150°W-90°W] delineated in blue in (h), respectively) for the individual NMME model's ensemble average forecast (colored lines), the multi-model ensemble average forecast (thick black lines) and the observed indices for the 1997-98 and 2015-16 events (dashed black lines).

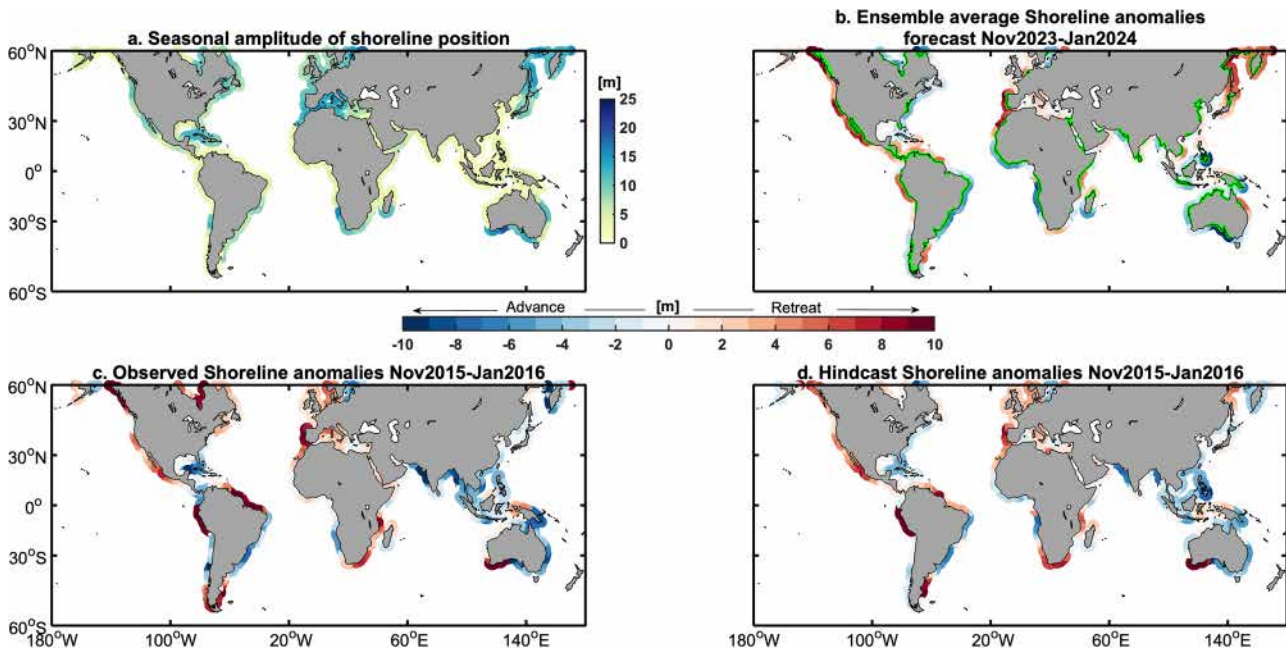


Fig. 2 Waterline position anomalies forecasts. **a** Amplitude in meters of seasonal variations in global coastal waterline position from a dataset of satellite-derived monthly waterline spanning the period 1999 to 2019. **b** Ensemble average predictions of anomalies (in m) in the waterline positions (November 2023 - January 2024 mean) using the model (Eq. 1) trained for the period 1999–2019 and for an ensemble of predictions constructed with the Niño3 and Niño4 monthly values from the NMME multi-model ensemble forecasts (first row of Supplementary Table 1) and 1000 different monthly values of each climate index (Indian Ocean Dipole, Southern Annular Mode, and North Atlantic Oscillation) covering their historical variations. Green dots in Fig. 2b indicate predictions that are significant with respect to seasonal amplitude (predictions greater or less than half the seasonal variation) and to non-ENSO climate variability, i.e., if the spread (\pm one standard deviation, cf. Supplementary Fig. 1) of the predicted waterline anomalies remains of the same sign across all values of the other climate mode indices. This indicates locations where the waterline is consistently retreating or advancing, independent of natural climate variability in other basins, and where such changes are substantial compared to normal annual variations. Overall, our predictions tend to remain significant in the tropical belt, where the influence of ENSO is dominant and natural seasonal variations in waterline positions remain small. For comparison, Fig. 2c, d shows the respectively observed and simulated anomalies during the last El Niño event in 2015–16, which shares commonalities with the upcoming one. Following the expected seesaw pattern of SLA (Supplementary Fig. 2a–c) and wave anomalies (Supplementary Fig. 2d–f) across the Pacific associated with El Niño, our projections evidence an important waterline retreat in the eastern Pacific and relative advance in the Indo-Pacific basin (including Australia). As the equatorward shift of the North Pacific storm track extends across the U.S. into the Atlantic, the associated increased wave activity and positive SLA tend to promote waterline retreat along the southern European coasts, while Scandinavia and the U.S. East Coast are characterized by waterline advance due to decreased wave activity and negative SLA (Fig. 2b and Supplementary

Fig. 2f). The coastlines bordering the South Atlantic are generally characterized by waterline advance. Overall, such patterns resemble those of the 2015–16 El Niño although with smaller values because the upcoming event is expected to be weaker, thus characterized by weaker teleconnections. The main differences between the two events are found in the Southern Hemisphere (e.g., South Chile, Western Australia), which can be attributed to differences in wave activity due to SAM, whose seasonal mean values were strongly positive in 2015–16, while our ensemble average projection emphasizes the impact of El Niño alone (cf. Supplementary Fig. 3).

PERSPECTIVES

Uncertainty still surrounds the main ingredients that govern the evolution of El Niño. However, since the current forecasts are initialized beyond the predictability barrier, they are more skillful, and thus, this event is not likely to develop as a strong event like the 1997–98 El Niño. So far, its evolution in the equatorial Pacific resembles that of the 2015–16 El Niño, yet with distinct impact on the world’s coastal waterline, probably due to differences in global teleconnections and onsets (e.g., occurrence of a strong coastal El Niño off Peru in March–April 2023). Furthermore, the picture painted here of El Niño impacts on coastlines, including potential flooding and erosion risks, is based on a simple data-driven model and a relatively coarse-resolution global dataset of waterline positions inferred from optical satellite imagery, in which some regions are inherently characterized by low signal-to-noise ratios. The amplitude of predicted anomalies should thus be taken with caution. In particular, it cannot be taken as a given for predicting the evolution of (your) local beach, where small-scale

dynamics and local effects can drastically alter the regional outlook. Nevertheless, we believe that this approach can provide a general sense of the expected regional coastlines patterns driven by El Niño, from which a storyline approach can be implemented to address risk assessment on relevant coastal ecosystem services.

METHODS

Shoreline dataset

This study used a comprehensive global waterline dataset that was resampled using transects spaced at 0.5° (~ 50 km), following the same approach as ref. ³⁵, effectively covering approximately 1.5 million kilometers. The initial coastline dataset used was the Global Self-consistent Hierarchical High-resolution Geography (GSHHG version 2.3.6124³⁷), which facilitated the identification of locations along the world's coastlines. Multiple satellite acquisitions from Landsat missions 5, 7, and 8 were used to derive monthly composites of the coastal waterline as a proxy of shoreline positions from 1993 to 2019. Because of the multiple re-passages of satellite after the late 1990s, we restricted the study period to January 1999 until December 2019. Satellite images were used to generate Normal Difference Water Index (NDWI) maps, with an NDWI threshold set at 0. This method identified pixels corresponding to ocean surfaces for $NDWI > 0$, and land surfaces for $NDWI < 0$ ³⁸. The shoreline/waterline was then accurately identified as the interface between these land and ocean surfaces. Contrary to a shoreline defined as a given coastal elevation (i.e., a given topography isoline), a waterline (water limit) evolves under potential morphological changes but also by coastal water level fluctuations that can be driven by waves, large- and local-scale sea-level variability and river freshwater flow. Compared to the dataset used in ref. ³³ in this version

1. We used a buffer zone, 500 m and 2000m cross-shore and along-shore, respectively, to get rid of outliers.
2. Then all points within this buffer zone are projected onto the cross-shore transect and linearly interpolated over time, with a running average over 3 months.
3. Finally, all transects are aggregated using a 4-degree spatial smoothing to average the waterline position.

Seasonal predictions

We used the SST anomaly outputs of seasonal forecasts from the North American Multi-model Ensemble project (NMME) project, a multi-model forecast system that includes models from the operational forecast centers in the United States and Canada⁷.

Climate-based model for interannual evolution of waterline positions

The 3-months detrended monthly *waterline* interannual anomaly (cleared from the monthly mean climatology) S is then formulated as:

$$S(x, t) = F(ENSO) + \varepsilon(x)NAO + \zeta(x)SAM + \eta(x)IOD, \quad (1)$$

With $F(ENSO) = A(x)Nino3 + B(x)Nino4$

$$+ (C(x)Nino3 + D(x)Nino4) * \cos\left(\frac{2\pi(t - \phi)}{12}\right) \quad (2)$$

Where x and t represent the along-shore and temporal dimensions, respectively, with 0.5° alongshore and monthly resolution, respectively, and the phase $\phi = 1$ (i.e., January) so that ENSO is peaking in December-February. Again, the reader is invited to refer ref. ³⁵ for more details about the design of the model. The model's coefficients ($A(x)$, $B(x)$, $C(x)$, $D(x)$, $\varepsilon(x)$, $\zeta(x)$ and $\eta(x)$) have been inferred through multiple linear regression over the period 1999–2019.

To distinguish the El Niño Southern Oscillation (ENSO) from other climate modes, we consider the Indian Ocean Dipole (IOD), the Southern Annular Mode (SAM) in the Southern Hemisphere, and the North Atlantic Oscillation (NAO) in the Northern Hemisphere. The SAM index is derived from the zonal pressure difference between mid-latitudes ($40^\circ S$) and higher latitudes ($65^\circ S$) in the Southern Hemisphere. Meanwhile, the NAO index is calculated from the difference in pressure at sea level between the subpolar low in Iceland and the subtropical high in the Azores. As for the IOD, it is characterized by an anomalous sea surface temperature (SST) gradient between the western equatorial Indian Ocean ($50^\circ E$ – $70^\circ E$ and $10^\circ S$ – $10^\circ N$) and the southeastern equatorial Indian Ocean ($90^\circ E$ – $110^\circ E$ and $10^\circ S$ – $0^\circ N$). Linear detrending was applied to all climate indices, and the seasonal cycle was removed using a monthly mean seasonal climatology. This process allows us to focus on the inter-annual variability, which was further smoothed using a running mean with a 3-month window over the period 1999–2019. This approach allows us to effectively analyze the fluctuations and patterns associated with the interannual variations of these climate modes, while minimizing the influence of long-term trends and seasonal variations. All climate indices are downloaded from the NOAA portal (<https://psl.noaa.gov/data/climateindices/list/>).

DATA AVAILABILITY

The waterline data are available upon request to rafael.almar@ird.fr. The climate indices are available on the data portal: <https://psl.noaa.gov/data/climateindices/list/>. The forecasts from the NMME are available on the portal: https://ftp.cpc.ncep.noaa.gov/NMME/realtime_anom/

CODE AVAILABILITY

The codes are available upon request to julien.boucharel@ird.fr.

Received: 28 August 2023; Accepted: 7 January 2024;

Published online: 06 February 2024

REFERENCES

1. McPhaden, M. J., Zebiak, S. E. & Glantz, M. H. ENSO as an integrating concept in earth science. *Science* **314**, 1740–1745 (2006).
2. Nobre, G. G., Muis, S., Veldkamp, T. I. & Ward, P. J. Achieving the reduction of disaster risk by better predicting impacts of El Niño and La Niña. *Prog. Disaster Sci.* **2**, 100022 (2019).
3. Guilyardi, E. et al. Understanding El Niño in ocean–atmosphere general circulation models: Progress and challenges. *Bull. Am. Meteorol. Soc.* **90**, 325–40, (2009).
4. L'Heureux, et al. in *El Niño Southern Oscillation in a Changing Climate* (eds McPhaden, M., Santoso, A., Cai, W.) 253, 377 (American Geophysical Union, 2020).
5. Wang, Y. et al. An improved ENSO ensemble forecasting strategy based on multiple coupled model initialization parameters. *J. Adv. Model Earth Syst.* **11**, 2868–2878 (2019).
6. Liu, T., Song, X., Tang, Y., Shen, Z. & Tan, X. ENSO predictability over the past 137 years based on a CESM ensemble prediction system. *J. Clim.* **35**, 763–777 (2022).
7. Sharmila, S., Hendon, H., Alves, O., Weisheimer, A. & Balmaseda, M. Contrasting El Niño–La Niña predictability and prediction skill in 2-year reforecasts of the twentieth century. *J. Clim.* **36**, 1269–1285 (2023).
8. Kirtman, B. P. et al. The North American multimodel ensemble: phase-1 seasonal-to-interannual prediction; phase-2 toward developing intraseasonal prediction. *Bull. Am. Meteor. Soc.* **95**, 585–601 (2014).
9. Comunicado ENFEN no3-2023 <https://www.gob.pe/institucion/senamhi/colecciones/1308-comunicados-enfen>
10. Boucharel, J., Timmermann, A., & Jin F.-F., Zonal phase propagation of ENSO SST anomalies - revisited. *Geophys. Res. Lett.* <https://doi.org/10.1002/grl.50685> (2013).
11. Rasmusson, E. M. & Carpenter, T. H. Variations in tropical sea surface temperature and surface wind fields associated with the Southern Oscillation/El Niño. *Mon. Weather Rev.* **110**, 354–384 (1982).
12. Kao, H. J. & Yu, J. Y. Contrasting eastern-Pacific and central-Pacific types of ENSO. *J. Clim.* **22**, 615–632 (2009).
13. Kug, J. S. et al. El Niño: cold tongue El Niño and warm pool El Niño. *J. Clim.* **22**, 1499–1515 (2009).

14. Kovats, R. S., Bouma, M. J., Hajat, S., Worrall, E. & Haines, A. El Niño and health. *Lancet* **362**, 1481–1489 (2003).
15. Cinner, J. E. et al. Evaluating social and ecological vulnerability of coral reef fisheries to climate change. *PLoS One* **8**, e74321 (2013).
16. Burton, C. et al. El Niño driven changes in global fire 2015/16. *Front. Earth Sci.* **8**, 199 (2020).
17. Glantz, M. H. *Climate variability, climate change and fisheries* (Cambridge University Press, 2005).
18. Liu, Y. et al. Nonlinear El Niño impacts on the global economy under climate change. *Nat. Commun.* **14**, 5887 (2023).
19. Callahan, C. W. & Mankin, J. S. Persistent effect of El Niño on global economic growth. *Science* **380**, 1064–1069 (2023).
20. Barnard, P. L. et al. Extreme oceanographic forcing and coastal response due to the 2015–2016 El Niño. *Nat. Commun.* **8**, 14365 (2017).
21. Vos, K., Harley, M. D., Turner, I. L. & Splinter, K. D. Pacific shoreline erosion and accretion patterns controlled by El Niño/Southern Oscillation. *Nat. Geosci.* **16**, 140–146 (2023).
22. Ranasinghe, R., McLoughlin, R., Short, A. & Symonds, G. The Southern oscillation index, wave climate, and beach rotation. *Mar. Geol.* **204**, 273–287 (2004).
23. Harley, M., Turner, I., Short, A. D. & Ranasinghe, R. Inter-annual variability and controls of the Sydney wave climate. *Int. J. Climatol.* **30**, 1322–1335 (2010).
24. Barnard, P. L. et al. Coastal vulnerability across the Pacific dominated by El Niño/Southern Oscillation. *Nat. Geosci.* **8**, 801–807 (2015).
25. Storlazzi, C. D. & Gary, B. G. Influence of El Niño–Southern Oscillation (ENSO) events on the coastline of central California. *J. Coastal Res.* 146–153 (1998).
26. Biribo, N. & Woodroffe, C. D. Historical area and shoreline change of reef islands around Tarawa Atoll, Kiribati. *Sustain. Sci.* **8**, 345–362 (2013).
27. Barnard, P. L., et al. The impact of the 2009–10 El Niño Modoki on US West Coast beaches. *Geophys. Res. Lett.* <https://doi.org/10.1029/2011GL047707> (2011).
28. Young, A. P. et al. Southern California coastal response to the 2015–2016 El Niño. *J. Geophys. Res. Earth Surf.* **123**, 3069–3083 (2018).
29. Cuttler, M. V. et al. Interannual response of reef islands to climate-driven variations in water level and wave climate. *Remote Sens.* **12**, 4089 (2020).
30. Duke, N. C. et al. ENSO-driven extreme oscillations in mean sea level destabilise critical shoreline mangroves—An emerging threat. *PLoS Clim.* **1**, e0000037 (2022).
31. Timmermann, A., An, S.-I., Kug, J.-S. & Jin, F.-F. El Niño–southern oscillation complexity. *Nature* <https://doi.org/10.1038/s41586-018-0252-6> (2018).
32. Boucharel, J., Almar, R., Kestenare, E. & Jin, F.-F. On the influence of ENSO complexity on pan-pacific coastal wave extremes. *Proc. Natl Acad. Sci.* **118**, e2115599118 (2021).
33. Boucharel, J., David, M., Almar, R. and A. Melet. Contrasted influence of climate modes teleconnections to the interannual variability of coastal sea level components—implications for statistical forecasts. *Clim. Dyn.* <https://doi.org/10.1007/s00382-023-06771-1> (2023).
34. Boucharel, J., Santiago, L., Almar, R. & Kestenare, E. Coastal wave extremes around the Pacific and their remote seasonal connection to climate modes. *Climate* **9**, 168 (2021).
35. Almar, R. et al. Influence of El Niño on the variability of global shoreline position. *Nat. Commun.* **14**, 3133 (2023).
36. Stuecker, M. et al. A combination mode of the annual cycle and the El Niño/Southern Oscillation. *Nat. Geosci.* **6**, 540–544 (2013).
37. Wessel, P. & Smith, W. H. F. A global self-consistent, hierarchical, high-resolution shoreline database. *J. Geophys. Res.* **101**, 8741–8743 (1996).
38. Kelly, J. T. & Gontz, A. M. Using GPS-surveyed intertidal zones to determine the validity of shorelines automatically mapped by Landsat water indices. *Int. J. Appl. Earth Obs. Geoinf.* **65**, 92–104 (2018).

ACKNOWLEDGEMENTS

B.D. acknowledges support from Agencia Nacional de Investigación y Desarrollo (Concurso de Fortalecimiento al Desarrollo Científico de Centros Regionales 2020-R20F0008-CEAZA and Fondecyt Regular grant 1231174) and the LEFE-GMMC (SEPICAF project). R.A. is funded by the French ANR through the project GLOBCOASTS (ANR-22-ASTR-0013 GLOBCOASTS).

AUTHOR CONTRIBUTIONS

J.B. and R.A. designed and conceptualized the study. J.B. conducted the analysis and wrote the initial version of the manuscript. All authors discussed the results and contributed writing the manuscript.

COMPETING INTERESTS

The authors declare no competing interests.

ADDITIONAL INFORMATION

Supplementary information The online version contains supplementary material available at <https://doi.org/10.1038/s41612-024-00570-z>.

Correspondence and requests for materials should be addressed to Julien Boucharel or Rafael Almar.

Reprints and permission information is available at <http://www.nature.com/reprints>

Publisher's note Springer Nature remains neutral with regard to jurisdictional claims in published maps and institutional affiliations.



Open Access This article is licensed under a Creative Commons Attribution 4.0 International License, which permits use, sharing, adaptation, distribution and reproduction in any medium or format, as long as you give appropriate credit to the original author(s) and the source, provide a link to the Creative Commons license, and indicate if changes were made. The images or other third party material in this article are included in the article's Creative Commons license, unless indicated otherwise in a credit line to the material. If material is not included in the article's Creative Commons license and your intended use is not permitted by statutory regulation or exceeds the permitted use, you will need to obtain permission directly from the copyright holder. To view a copy of this license, visit <http://creativecommons.org/licenses/by/4.0/>.

© The Author(s) 2024